PNAS Nexus, 2024, 3, pgae444
https://doi.org/10.1093/pnasnexus/pgae444
Advance access publication 4 October 2024
Research Report

Position-dependent roles of somatic cells in phototaxis of *Volvox*

Keigo Harada[a], Yukariko Komasaka[a], Keisuke Yamada[a], Takumi Iizuka[a], Minato Otani[a] and Yoshihiro Murayama[a,b,*]

[a]Department of Applied Physics, Tokyo University of Agriculture and Technology, Koganei, Tokyo 184-8588, Japan
[b]Department of Biomedical Engineering, Tokyo University of Agriculture and Technology, Koganei, Tokyo 184-8588, Japan
*To whom correspondence should be addressed: Email: ymura@cc.tuat.ac.jp
Edited By Eva Kanso

Abstract

A spherical green alga, *Volvox*, achieves phototaxis via a simple on/off switch of flagellar beating in response to changes in light intensity, without the need for complex signal transduction between cells. Moreover, the alga can change its susceptibility to light in order to adapt to its environment. To identify the mechanisms of susceptibility regulation, experiments were conducted at three different levels: population, individual, and cellular. The light intensity dependence of the average velocity at the population level and that of the change in flow speed obtained at the individual level were consistent, indicating that susceptibility regulation occurred in each *Volvox* colony. Furthermore, by measuring the probability of stopping flagellar beating when the light intensity was changed, susceptibility regulation was found to result from the properties of somatic cells as differential and adaptive photosensors. These photosensing properties deteriorated from the anterior to the posterior regions of the colony. Considering the mechanical motion of a *Volvox* colony, the position-dependent ability of somatic cells indicates that the anterior cells play the role of a rudder, whereas the posterior cells play the role of a rower. The position-dependent properties of somatic cells imply an early stage of cell differentiation that allows for an efficient response to changes in the circumstances.

Keywords: *Volvox*, phototaxis, susceptibility, adaptation

Significance Statement

Microorganisms often achieve functional motions in a simple manner. A spherical green alga, *Volvox*, consisting of thousands of somatic cells, can detect differences in light intensity and swim toward bright areas. Furthermore, this alga can change its susceptibility to light by adapting to the environmental light intensity. In this study, each cell was found to be equipped with an adaptive mechanism whose function depended on the position of the somatic cells. Position-dependent properties are indicative of early stages of cell differentiation. This simple but sophisticated regulation mechanism is a source of inspiration for the development of technologies such as microrobots and automated regulation systems.

Introduction

Living organisms can sense their surroundings and adapt to environmental changes in their circumstances. Multicellular organisms, which consist of many differentiated cells, often realize the adaptation using complex signal transduction between cells. However, relatively simple microorganisms also realize functional motion and adaptation through sophisticated strategies, without the need for complex signal transduction or the nervous system (1–5). The simple and functional mechanisms of microorganisms have inspired the development of soft micromachines (6) and biohybrid machines (7–9).

The spherical green alga *Volvox* also shows functional motion in phototaxis (10–12), with a flagellar photoresponse that depends on the species (13, 14). *Volvox* has been studied as a model organism for development, morphogenesis, and multicellularity (15–19). Its spherical shape and flagellar motion have also attracted the attention of researchers in the field of fluid dynamics (20–24). An individual colony of *Volvox* consists of thousands of somatic cells on its surface and a small number of germ cells inside the sphere. The germ cells grow into daughter colonies and hatch from the mother colony over a 48-h period. As shown in Fig. 1A, a *Volvox* colony has an anterior–posterior (a–p) axis, with daughter colonies located at the rear, causing bottom-heaviness; therefore, the colony turns upward against gravity. Each somatic cell on the surface has an eyespot (Fig. 1B) and two flagella (Fig. 1C). The eyespot acts as a directional light sensor, and the flagellar beatings are controlled by Ca^{2+} concentration (25–29). As the direction of flagellar beating is slightly tilted longitudinally,

Competing Interest: The authors declare no conflict of interests.
Received: June 4, 2024. **Accepted:** September 20, 2024

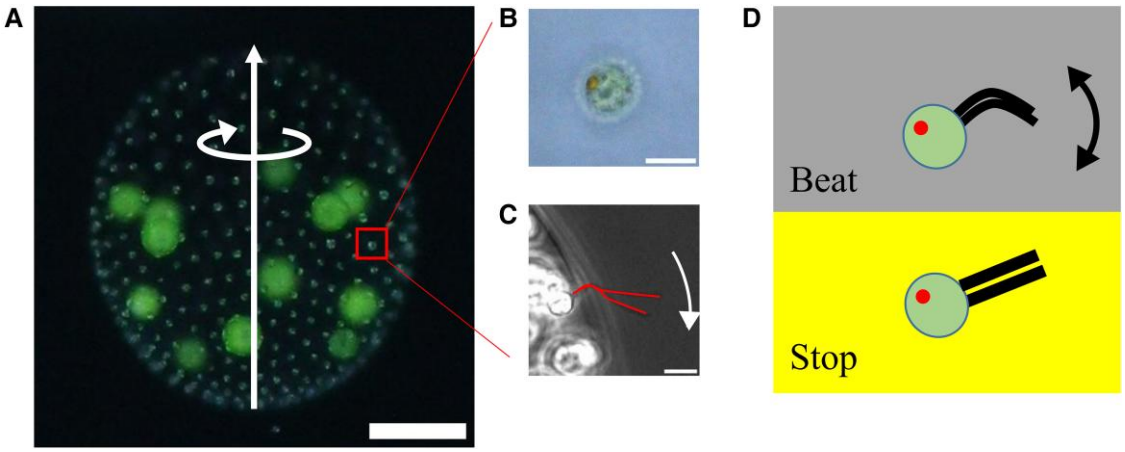

Fig. 1. A) A *Volvox* colony. Small dots indicate somatic cells, while the large circles in the rear are daughter colonies. The a–p axis is denoted by a straight arrow. The colony rotated counterclockwise around a–p axis. Scale bar = 100 μm. B) Somatic cell with an eyespot. Scale bar = 10 μm. C) Two flagella equipped on a somatic cell. Scale bar = 10 μm. D) Beat and stop modes of the flagellar states.

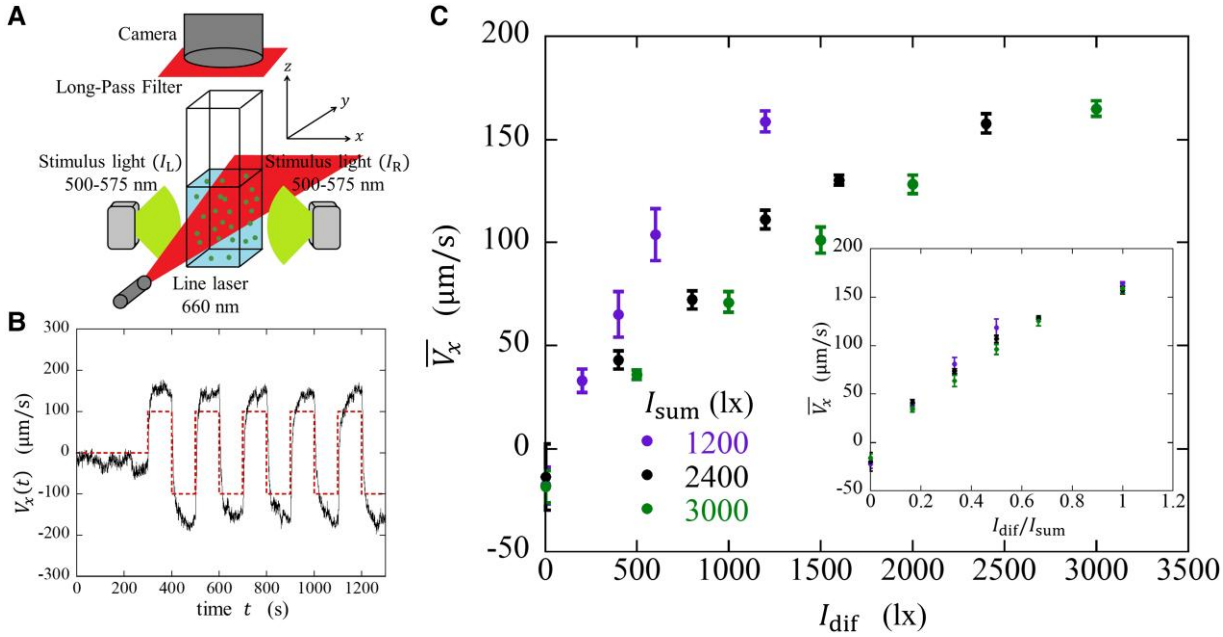

Fig. 2. A) Schematics of experimental setup for the measurement at colony population level. *Volvox* colonies within a thickness of 1–2 mm of the line laser were observed from the top. B) $V_x(t)$ for $I_{dif} = \pm 2{,}400$ lx and $I_{sum} = 2{,}400$ lx. Dotted line represents the rectangular light stimulus. C) $\overline{V_x}$ against I_{dif} for $I_{sum} =$ 1,200, 2,400, and 3,000 lx. Mean values and standard errors for five trials are plotted. Inset: Same data are plotted against I_{dif}/I_{sum}.

the colony swims forward and spins counterclockwise when viewed from behind.

The phototaxis of the *Volvox* is achieved in a simple and sophisticated manner (30). When the eyespot of a somatic cell detects a change in light intensity from dark to bright, the flagella of the somatic cell stop beating for a few seconds before recovering (Fig. 1D). When the colony is illuminated from one side, its rotation creates an area on the bright side where flagellar beating stops; this area becomes larger as the rotation speed increases or the recovery time of the beating is prolonged. This flagellar stopping area causes a torque that tilts the a–p axis toward the light source, breaking the initial torque balance. The tilting continues until the torque from the flagellar stopping balances with the torque caused by the bottom-heaviness. As a result, the *Volvox* colony swims toward the bright side.

In our previous study (31), we illuminated *Volvox* colonies from the right and left sides of a chamber with I_R and I_L light intensities and found that they responded to the light intensity difference, $I_{dif} = I_R - I_L$. Furthermore, the velocity component along the light stimulus axis was uniquely determined by the relative light intensity difference, I_{dif}/I_{sum}, where $I_{sum} = I_R + I_L$. These results indicate that, as a simple organism without signal transduction between cells, *Volvox* can change its susceptibility to adapt to the light intensity of the environment, similar to organisms with complex signal transduction. Although the mechanism by which this susceptibility to light is regulated remains unclear, it may be achieved by the integration of several 1,000 cells, or each cell may be equipped with its regulatory mechanism. To identify the factors that play a role in the mechanism responsible for the regulation of susceptibility, experiments were conducted at three

levels: population, individual, and cellular. The results showed that each somatic cell can act as a differential and adaptive sensor to differences in light intensity and that this ability varies with the position of the cell, with a higher ability near the front. These position-dependent roles of somatic cells can lead to efficient responses to changes in environmental conditions such as variations in light intensity, flow direction, or other factors that disturb their movement direction.

Results

Photoresponses of the *Volvox* colony population

First, we measured the photoresponses of *Volvox* at the population level using our modified setup to confirm the previous results (31) and evaluate responses to differences in light intensity. A schematic of the experimental setup is shown in Fig. 2A. We observed the motion of *Volvox* in the *xy*-plane under a rectangular light stimulus along the *x*-axis. We changed $I_{dif} = I_R - I_L$ for a given $I_{sum} = I_R + I_L$ and obtained the average velocity on the *x*-axis, $V_x(t)$, for the colonies at time *t*. Figure 2B shows a typical $V_x(t)$, indicating the response to a rectangular stimulus. Using time-series analysis, we calculated the mean value of $\overline{V_x}$ over time for five rectangular stimuli in a trial. Further details are provided in the Materials and methods.

Figure 2C shows $\overline{V_x}$ vs. I_{dif} for I_{sum} = 1,200, 2,400, and 3,000 l×. $\overline{V_x}$ increased with an increasing I_{dif}. The small negative values of $\overline{V_x}$ at $I_{dif} = 0$ may result from slight differences between I_R and I_L owing to the illumination setup. A similar trend was observed for $\cos\phi$, where ϕ is an angle from the *x*-axis, which indicates that the colonies tended to be directed to the light source with an increasing I_{dif} (Fig. S1). Moreover, the data for different I_{sum} values collapsed into a single curve when plotted against I_{dif}/I_{sum}, as shown in Fig. 2C (inset). These results are consistent with our previous findings (31), suggesting that *Volvox* adjusts its susceptibility to I_{dif}, increasing it under dark conditions and decreasing it under bright conditions.

Flow around an individual *Volvox* colony

Next, to determine whether the regulation of susceptibility to light was driven by an individual *Volvox* colony, we measured the flow speed around the colony under light stimuli, with reference to the literature (30). Figure 3A shows a schematic of the experimental setup. A *Volvox* colony was immobilized by aspiration using a glass micropipette, and particle-tracking velocimetry (PTV) was conducted on the tracer particles in a rectangular area in front of the colony, as shown in Fig. 3B. In this experiment, the light intensity was changed from I_{before} to I_{after}, where we regarded $I_{after} - I_{before}$ as I_{dif}, and $I_{after} + I_{before}$ as I_{sum}. Further details are provided in the Materials and methods.

Figure 3C shows a typical time series of the flow speed, $u(t)$. At t = 10 s, the light intensity changed from I_{before} to I_{after}. The flow speed rapidly decreased owing to the stoppage of flagellar beating and gradually recovered to a steady-state speed, as reported previously (30). We calculated the mean speed for t = 85 – 110 s as a steady speed u_0, and the time series of the recovery process was fitted by the curve $\frac{u(t')}{u_0} = 1 - \mathrm{Re}^{-t'/\tau_a}$, where t' is a time after the recovery process started, as shown in Fig. 3C (inset). *R* and τ_a are fitting parameters and indicate the decreasing rate of the flow speed and the characteristic time for the recovery, respectively. Figure 4A and B shows the I_{dif} dependence of *R* and τ_a, respectively. *R* increased with increasing I_{dif}, and the data collapsed into a single curve when plotted against I_{dif}/I_{sum} (inset). These results indicate that the susceptibility regulatory mechanism is equipped on an individual *Volvox* colony, rather than on a population. This trend was also observed for τ_a; however, the data did not collapse against I_{dif}/I_{sum} compared with that for *R*. Although *R* and τ_a exhibited similar dependence on I_{sum}, careful discussion is needed to reveal the underlying mechanisms. An increase in *R* and τ_a is indicative of an increase in the stop rate of flagellar beatings, which induce torque to change the direction of the colony toward the source of light. Thus, the alignment between the I_{dif}/I_{sum} dependencies shown in Figs. 2C and 4 is reasonable.

Measuring the stop probability of flagellar beatings

As reported in a previous study (30), the size of the eye spot decreases as the angle θ from the anterior pole increases, whereas the flagellar response decreases with an increase in θ; the flagellum at $\theta > 90°$ shows no response to the light stimulus. Thus, we investigated the dependence of the stop probability of flagellar beatings on I_{dif}, I_{sum}, and θ. The experimental setup was similar to that used for the flow measurements; further details are provided in the Materials and methods section. The angle θ was determined from the superimposed images (Fig. 5A). To determine the probability of stopping flagellar beating, we measured the mean illuminance of the 3 × 3 pixel grayscale (0–255) image near the flagellum (Fig. 5B). The illuminance showed large deviations when the flagellum was beating, and small deviations when it was stopped (Fig. 5C). To discriminate between the beating and stopping actions, we calculated the moving standard deviation of the illuminance over a window of 100 frames (Fig. 5D), which corresponded to 100 ms. As a result, flagellar motion was binarized into two states: beat (0) or stop (1) (Fig. 5E). The threshold value for the standard deviation of each plot was determined visually by careful observation of the graphs. Next, the moving average of the binarized results was calculated over 1,000 frames (1 s) to determine P_{1s}, which represented the stop probability with a time resolution of 1 s. Figure 5F shows the time series of P_{1s}. The stimulus light was changed from dark to bright at t = 10 s. Notably, flagellar beating stopped as a result of the changes in light intensity but resumed after a few seconds. In most cases, P_{1s} reached a maximum within 3 s after a change in the light intensity and then decayed (Fig. S2). The increase in P_{1s} resulted from the stopping of flagella, whereas the decrease resulted from recovery. Consequently, we defined the stop probability P_{stop} as the mean value of P_{1s} from 10 to 13 s.

The I_{dif} dependence of P_{stop} for somatic cells located at $\theta = 0 - 30$, $30 - 60$, and $60 - 90°$ is shown in Fig. 6A, C, and E, respectively, and the same data are plotted against I_{dif}/I_{sum} in Fig. 6B, D, and F. In the case of $\theta = 0 - 30°$, for all I_{sum}, P_{stop} increased as I_{dif} increased (Fig. 6A). Moreover, the slope decreased as I_{sum} increased. When the same data were plotted against I_{dif}/I_{sum}, they approximately collapsed into a single line, except I_{sum} = 9, 000 l×, as shown in Fig. 6B. These results indicate that the P_{stop} of anterior somatic cells at $\theta = 0 - 30°$ is determined by I_{dif}/I_{sum}. The anterior somatic cells showed an adaptive response to light stimuli up to I_{sum} = 5, 100 l×. Next, in the case of $\theta = 30 - 60°$, similar to the case of $\theta = 0 - 30°$, the P_{stop} increased as I_{dif} increased, as shown in Fig. 6C; however, the data collapsed in the plot against I_{dif}/I_{sum} was observed only for I_{sum} = 1, 200, 2, 400, and 3, 600 l×. Third, in the case of $\theta = 60 - 90°$, the values of P_{stop} were <0.05 for $I_{dif} < 2,000$ l× for all I_{sum}, as shown in Fig. 6E. For $I_{dif} \geq 2,000$ l×, the P_{stop} increased as I_{dif} increased; however, it is worth noting that the P_{stop} was determined by I_{dif} rather than I_{dif}/I_{sum}, comparing between Fig. 6E and F. To

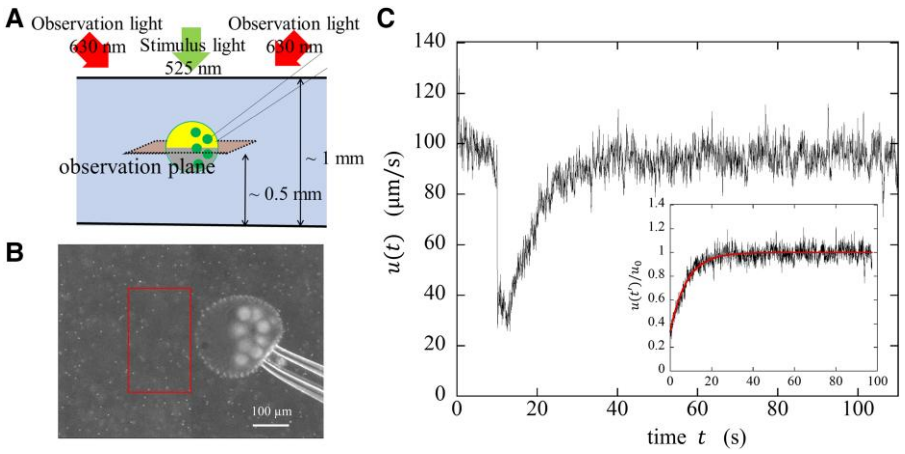

Fig. 3. A) Experimental setup for measurement at the individual level. B) Snapshot of the PTV image. The rectangular is the area for PTV analysis. C) Time series of flow speed $u(t)$. Light stimulus was applied at t = 10 s. Inset: Time series of $u(t')/u_0$. The solid curve is a fitting curve.

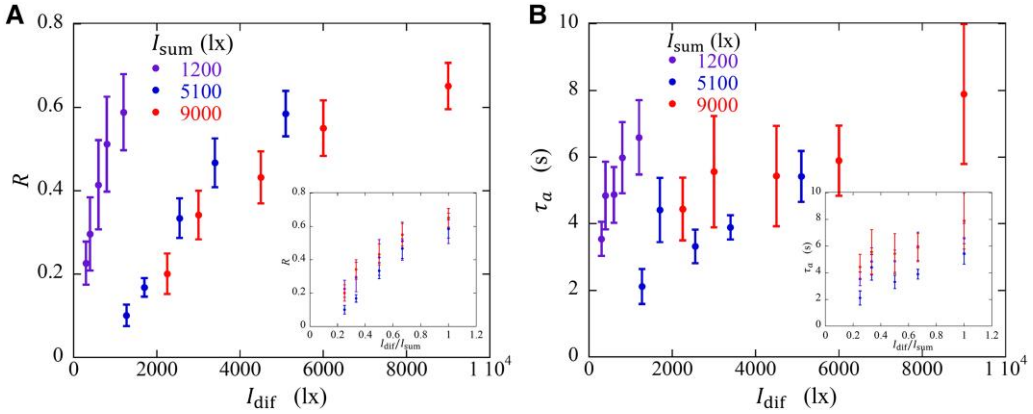

Fig. 4. I_{dif} and I_{dif}/I_{sum} (inset) dependence of R (A) and τ_a (B) for I_{sum}=1,200, 5,100, and 9,000 lx, obtained from flow measurements around a *Volvox* colony under light stimuli. The mean values and standard errors of the six colonies were plotted.

summarize, (i) P_{stop} increased as I_{dif} increased when the somatic cell responded to the light stimulus; (ii) somatic cells at $\theta = 0 - 30°$ showed an adaptive response to the I_{sum} for $I_{sum} \leq 5,100$ lx; (iii) somatic cells at $\theta = 30 - 60°$ showed an adaptive response to the I_{sum} for $I_{sum} \leq 3,600$ lx; (iv) somatic cells at $\theta = 60 - 90°$ showed approximately no response to the $I_{dif} < 2,000$ lx and no adaptive response to the I_{sum}. To identify the photosensing properties of somatic cells, the same data in Fig. 6 were compared between θ for a given I_{sum} (Fig. S3), and for a given I_{dif}/I_{sum} (Fig. S4).

These results suggest that the somatic cells of *Volvox* exhibit the following photosensing properties: (i) differential sensor in response to I_{dif}; (ii) adaptive sensor to adapt to the magnitude of I_{dif}; (iii) a decreasing ability of (i) and (ii) with an increasing θ. This suggests that somatic cells adapt to the I_{dif} rather than I_{sum} because they respond to changes in light intensity. Property (iii) implies that somatic cells have a range of responses and adaptations to the I_{dif}. In this experiment, the light intensity was changed from I_{before} to I_{after}. From the definition of I_{sum}, the light intensity was varied, satisfying the relation $I_{after} = -I_{before} + I_{sum}$ for a given I_{sum}. The findings suggest that somatic cells had a lower limit I_{dif}^{min} for their response and an upper limit I_{dif}^{max} for their adaptation in I_{dif}, depending on θ, as shown in Table 1. Somatic cells have the ability to act as a differential sensor in the range $I_{after} > I_{before} + I_{dif}^{min}$, and as an adaptive sensor in the range $I_{after} < I_{before} + I_{dif}^{max}$. These ranges were wide for anterior somatic cells, and the cells at $\theta = 60 - 90°$ could not respond or adapt to small differences in light intensity (<2, 000 lx). The position-dependent ability correlated with the size of the eye spot, which became smaller with increased θ (30). In our measurements, *Volvox* colonies with an a–p axis in the xy-plane were selected, and the stimulus light was applied from above. Because the outermost somatic cells were observed, the orientations of eye spots relative to the stimulus light were consistent regardless of θ. Therefore, any position-dependent effect is likely attributable to the eyespot size.

How is the direction of motion of *Volvox* determined?

From experiments conducted at three different levels, each somatic cell was found to act as a differential and adaptive sensor for differences in light intensity. This ability was found to be highest in anterior cells. In this section, we discuss the direction of the a–p axis and colony motion with reference to a previous study (30).

Because the Reynolds number for a swimming *Volvox* colony is <0.01, the inertial contribution can be neglected in the equation of motion. Thus, the translational velocity of a colony is expressed as

$$\boldsymbol{v} = \frac{1}{\gamma_{trans}}(\boldsymbol{F} + \boldsymbol{F}_g), \quad (1)$$

where γ_{trans} is the viscosity coefficient, $\boldsymbol{F}$ is the net force due to flagella, and $\boldsymbol{F}_g$ is the force due to gravity. Assuming $\boldsymbol{F}_0$ is the force at which all somatic cells show no response to light, the colony

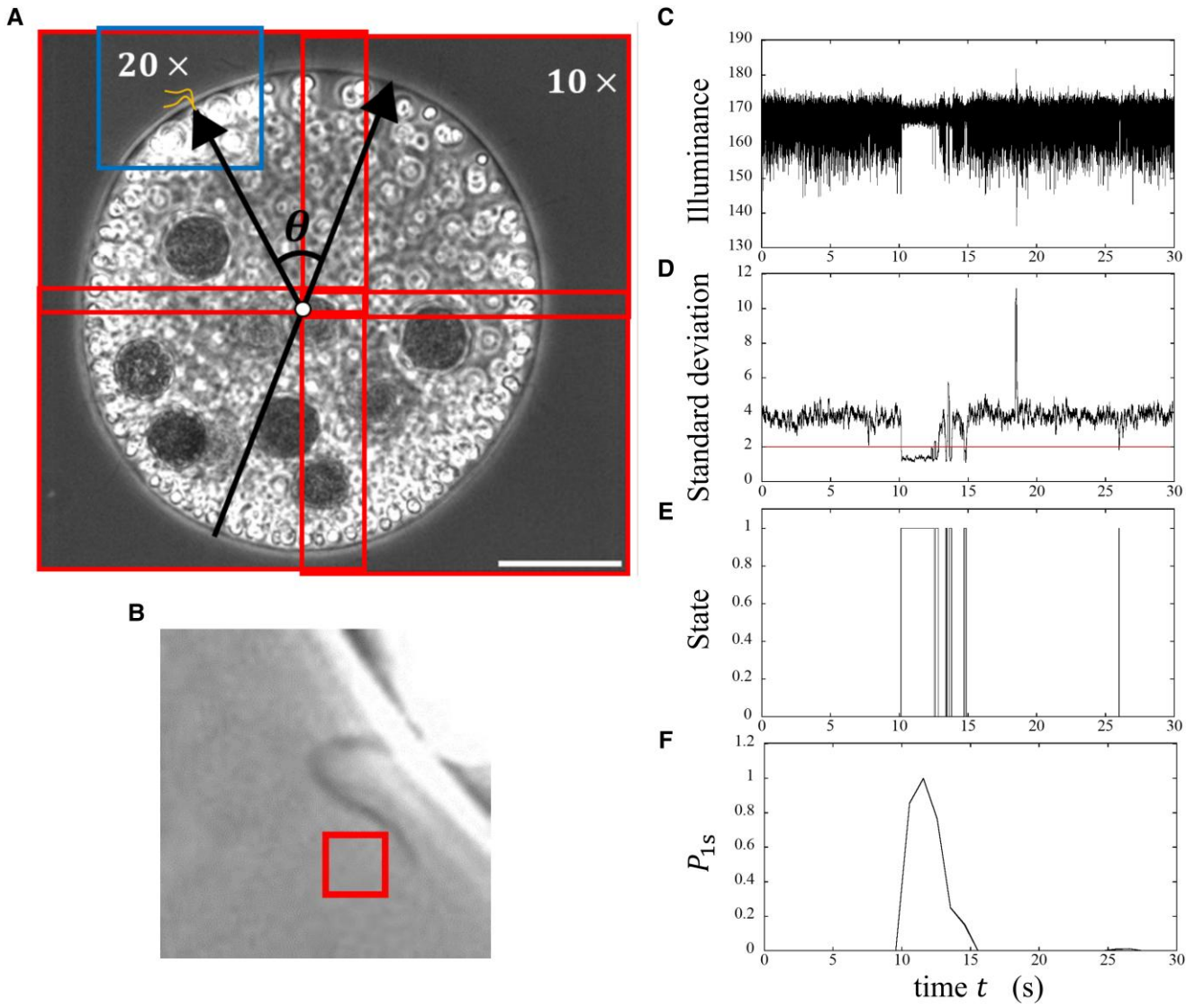

Fig. 5. A) Superimposed images of a *Volvox* colony. The 10× and 20× images are denoted by large and small rectangles, respectively. B) Magnified image of beating flagella. The rectangle indicates the 3 × 3 pixel area for measuring mean illuminance. C) Time series of the mean illuminance of the measured area. D) Time series of the moving standard deviation of the illuminance. E) Time series of the state of flagellar beating. 0 and 1 are beat and stop, respectively. F) Time series of P_{1s}.

moves in the direction of $\mathbf{F}_0 + \mathbf{F}_g$. For the rotational motion, neglecting the contribution of inertia, the angular velocity around the a–p axis is expressed as follows:

$$\boldsymbol{\omega} = \frac{1}{\gamma_{\mathrm{rot}}}\mathbf{N}, \tag{2}$$

where γ_{rot} is the viscosity coefficient in rotation, and $\mathbf{N}$ is the net torque. When all somatic cells show no response to light, the longitudinal forces due to the flagella are balanced on the left and right sides of the a–p axis. The latitudinal forces add up in one direction, resulting in torque $\mathbf{N}_0$ around the a–p axis of the colony, which causes spinning motion. In contrast, when somatic cells respond to light and stop flagellar beating, the net force and torque become:

$$\mathbf{F} = \mathbf{F}_0 - \int_A \boldsymbol{f}\mathbf{dS}, \tag{3}$$

$$\mathbf{N} = \mathbf{N}_0 - \int_A (\boldsymbol{r}\times\boldsymbol{f})\mathbf{dS}, \tag{4}$$

where $\boldsymbol{f} = (f_\theta, f_\varphi)$ is the force per unit area, A is the area in which the somatic cells can response to light and stop flagellar beatings, and $\boldsymbol{r}$ is the position vector of the somatic cell. The integrals are surface integrals on the colony surface. Furthermore, considering each component of the force, the integral in Eq. (4) is divided into $\mathbf{N}_\theta$ and $\mathbf{N}_\varphi$. Here, $\mathbf{N}_\theta = \int_A (\boldsymbol{r}\times f_\theta \boldsymbol{n}_\theta)\mathbf{dS}$ results in a directional change of the a–p axis, and $\mathbf{N}_\varphi = \int_A (\boldsymbol{r}\times f_\varphi \boldsymbol{n}_\varphi)\mathbf{dS}$ leads to a decrease in the spinning motion around the a–p axis, where $\boldsymbol{n}_\theta$ and $\boldsymbol{n}_\varphi$ are unit vectors in each direction. In the case of $\mathbf{N}_\theta \neq 0$, the a–p axis is tilted from the vertical direction, resulting in a torque $\mathbf{N}_{\mathrm{BH}}$ due to bottom-heaviness. That is, when a *Volvox* colony is showing phototaxis in a steady state, the a–p axis tilts from the z-axis until $\mathbf{N}_{\mathrm{BH}} = \mathbf{N}_\theta$, and the colony moves in the direction of $\mathbf{F} + \mathbf{F}_g$. In this steady state, the angle between the a–p axis and z-axis is θ_z, while that between the projection of the a–p axis on the xy-plane and x-axis is ϕ, as shown in Fig. 7A.

With regards to how ϕ is determined, we denoted the direction vector of the a–p axis as $\boldsymbol{n}_{ap}$. A schematic of the projection of a

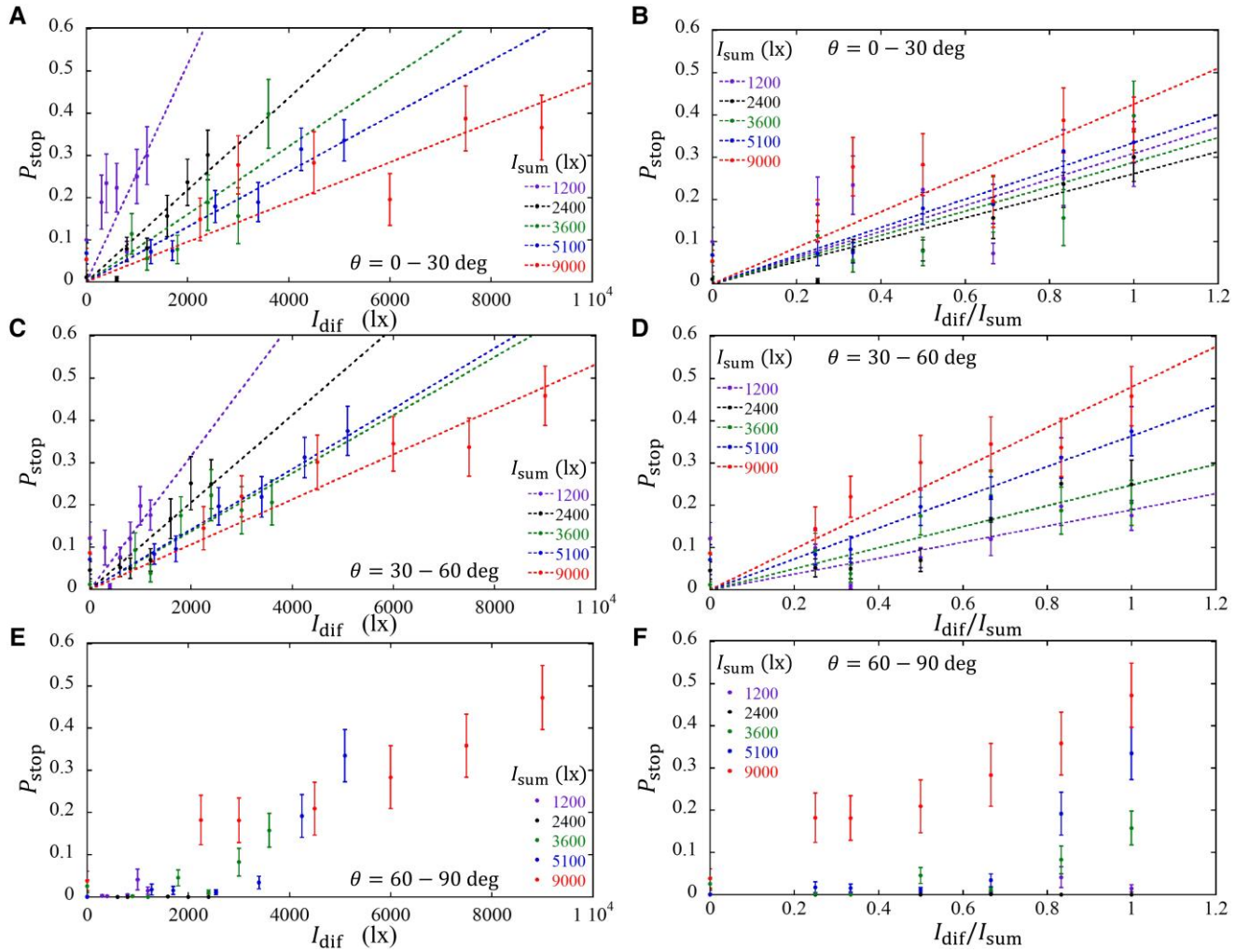

Fig. 6. I_{dif} (A, C, E) and I_{dif}/I_{sum} (B, D, F) dependence of P_{stop} for somatic cells located at $\theta = 0-30$, $30-60$, and $60-90°$. The mean values and standard errors for 8 – 14 somatic cells in 5 – 11 colonies are plotted. The dotted lines represent the linear fitting results.

Table 1. I_{dif} range for response and adaptation.

θ (°)	I_{dif} range for response (lx)	I_{dif} range for adaptation (lx)	I_{dif}^{min} (lx)	I_{dif}^{max} (lx)
0 – 30	$I_{dif} \leq 9,000$	$I_{dif} \leq 5,100 - 9,000$	0 – 300	5, 100 – 9, 000
30 – 60	$I_{dif} \leq 9,000$	$I_{dif} \leq 3,600 - 5,100$	0 – 300	3, 600 – 5, 100
60 – 90	$2,000 \leq I_{dif} \leq 9,000$	None	≈2, 000	None

300 and 9,000 lx represent the lower and upper limits of our experimental setup, respectively.

Volvox colony onto the xy-plane is shown in Fig. 7B. This figure assumes that the $\boldsymbol{n}_{ap}$ is initially parallel to the z-axis and that the colony is illuminated from the positive to the negative direction along the x-axis. As the colony is spinning, somatic cells stop flagellar beating at the border between the dark and bright sides of the colony surface. Area A, in which somatic cells stop flagellar beating, increases with time; however, the increase in A is limited by the recovery of flagellar beating. Assuming that τ_a is the duration for the flagellar stop and ω_s is the angular velocity in the steady state, $A \propto \omega_s \tau_a$. Therefore, if τ_a is shorter than half the period of the colony's spinning, $\boldsymbol{N}_\theta$ will be directed at an angle of $\pi - \frac{\omega_s \tau_a}{2}$ from the x-axis. Then, $\boldsymbol{n}_{ap}$ tilts to the direction of the angle $\phi = \frac{\pi}{2} - \frac{\omega_s \tau_a}{2}$, as shown in Fig. 7B. The value of ϕ decreases as τ_a increases; however, $\phi > 0$ as long as flagellar beating recovers when the somatic cell detects a change in light intensity from bright to dark. As shown in Fig. S1A, $\cos\phi \approx 0.5$ at $I_{dif}/I_{sum} = 0.33$, which indicates $\omega_s \tau_a \approx \pi/3$. Assuming ω_s is $\pi/3$ rad/s as a typical angular velocity of the colony's spinning, τ_a was estimated to be 1 s. This estimated value was slightly shorter than that shown in Fig. 4B, which might result from the stochastic behavior of the flagella stopping in each somatic cell.

Tilting the $\boldsymbol{n}_{ap}$ produces a midnight sun area around the anterior pole, where somatic cells detect no difference in light intensity during spinning (Fig. 7C). Thus, to balance between $\boldsymbol{N}_{BH}$ and $\boldsymbol{N}_\theta$, θ_z is $< \frac{\pi}{2}$, and area A needs to be in steady-state for phototaxis. It is worth noting that the direction of motion is $\boldsymbol{F} + \boldsymbol{F}_g$, different

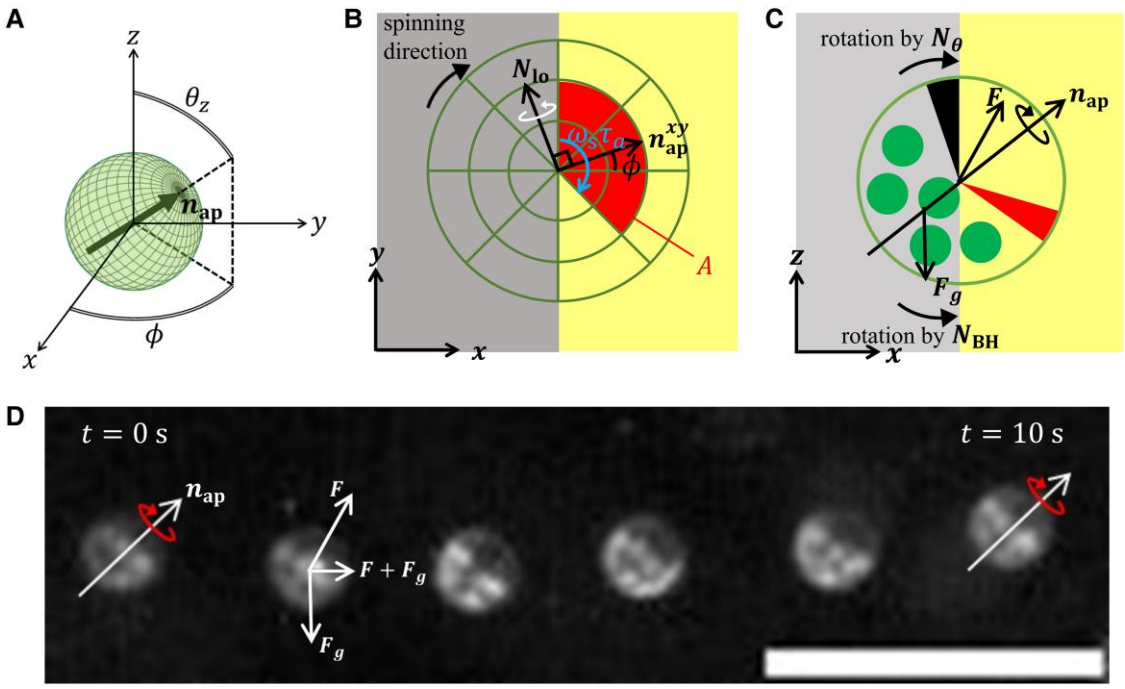

Fig. 7. A) *Volvox* colony showing phototaxis in steady state. B) Relationship between A, ω_s, τ_a, $\boldsymbol{n}_{ap}$, $\boldsymbol{N}_\theta$, and ϕ. $\boldsymbol{n}_{ap}^{xy}$ is the projection of $\boldsymbol{n}_{ap}$ onto the xy-plane in the steady state. C) Schematic view in the xz-plane in steady state in phototaxis. Somatic cells in the filled area on bright side generate $\boldsymbol{N}_\theta$ that balances with $\boldsymbol{N}_{BH}$. $\boldsymbol{F}$ due to flagellar beatings and $\boldsymbol{F}_g$ due to gravity determine the direction of motion of the colony. D) Motion of *Volvox* on the xz-plane, showing phototaxis. Curved arrow indicates the direction of spinning. The colony moves in approximately horizontal direction, not in the direction of the a–p axis. Scale bar = 1 mm.

from the direction of $\boldsymbol{n}_{ap}$. Figure 7D clearly shows the difference in direction between the a–p axis and motion.

Relationship between the photosensing properties of somatic cells and phototaxis of the colony

These results shed light on the position-dependent role of *Volvox* somatic cells in phototaxis. Assuming that the stop probability of flagella just after the change in the light intensity is $\hat{P}$, and the duration for the stop is τ_a, $|\boldsymbol{N}_\theta|$ is proportional to $\hat{P}\omega\tau_a$ because the area A is proportional to $\omega\tau_a$. On the other hand, P_{stop} defined in our measurements corresponds to $\hat{P}\tau_a$ because P_{stop} is the average valued during 3 s. The R in the flow measurements was assumed to correspond to $\hat{P}$. The increase in P_{stop} with an increase in I_{dif} contributes to an increase in $\boldsymbol{N}_\theta$, which causes an increase in θ_z and a decrease in ϕ.

For the *Volvox* colony shown in Fig. 7D, several interesting observations were made. Because θ_z is approximately 45°, somatic cells at $\theta > 30°$ are not able to detect a difference in light intensity. Thus, somatic cells at $30 < \theta\,(°) < 90$ produce $\boldsymbol{N}_\theta$ and realize the steady motion in phototaxis because somatic cells at $\theta > 60°$ show no adaptive response to I_{dif}. These results suggest that the somatic cells of *Volvox* play different roles depending on their positions. Somatic cells in the anterior part ($\theta < 30$ °) contribute to rapid changes in the direction of the a–p axis after detecting I_{dif}, those in the middle ($30 < \theta\,(°) < 60$) contribute to maintaining the steady motion in phototaxis, and those in posterior part ($\theta > 90$ °) produce the driving force for movement, independent of light intensity. In fact, the number density of cells increases from the anterior to the posterior, which suggests that a small number of cells are sufficient for the first rapid change in direction and that a large number of cells are needed to maintain translational motion. The direction of the a–p axis in nature is usually vertical because of the bottom-heaviness. However, when external flow or interaction with other objects perturbs the direction, the above position-dependent roles could be helpful in recovering the direction and rapidly moving to the most favorable areas. Although *Volvox* consists of two types of cells, somatic cells and germ cells, its position-dependent roles may be the first step in cell differentiation to achieve a higher-order function. Because we disregarded the effect of eyespot orientation with respect to incoming light in the present study, the actual role division among somatic cells is likely more gradual than that discussed above. For further consideration, a quantitative analysis of the contributions of somatic cells to colony motion is needed, which should include the effects of eyespot orientation and cell number density. Such quantitative analysis could explain the functional forms of $\overline{V_x}$ in Fig. 2C.

Conclusion

We found that the mechanism regulating the susceptibility of *Volvox* in phototaxis resulted from the properties of somatic cells as differential and adaptive photosensors. These results were consistent at the population, individual, and cellular levels. These photosensing properties deteriorated from the anterior to the posterior regions, suggesting that anterior cells act as rudders, whereas posterior cells act as rowers. Position-dependent cellular properties are considered signs of cell differentiation. Further studies are needed to investigate the relationships between role division and cell number using related green algae with a small number of cells, such as Gonium (8, 16 cells), Eudorina (16, 32 cells), and Pleodorina (64, 128 cells). The simple and sophisticated regulatory mechanism of *Volvox* highlighted in this study could be a source of inspiration for the development of technologies such as microrobots and automated regulation systems.

Materials and methods

Culture conditions

Volvox carteri Eve10 was grown in a natural medium consisting of 0.25 g of calcium carbonate, 0.25 mL of HYPONeX (commercial nutrient for plants, containing nitrogen, phosphorus, and potassium), and red soil in 350 mL of natural mineral water in a conical flask, in a daily cycle of 16 h in white light-emitting diode (LED) light (2,500–3,000 l×) and 8 h in the dark at 28 °C. After the culture was allowed to grow for 1–2 weeks, 25 mL of the *Volvox* solution was inoculated into the natural medium.

Measuring the photoresponses of a *Volvox* colony population

The experimental setup was approximately the same as that previously reported (31), comprising an $40 \times 40 \times 180$ mm^3 acrylic chamber that was illuminated by a line laser (2 mW/mm^2, Edmund Optics) at a wavelength of 660 ± 10 nm for observation. *Volvox* colonies showed negligible response to red light. Colonies within a thickness of 1–2 mm of the laser line were observed using a camera (ICL-B1410M; IMPERX). Briefly, 960×720 pixels images with a spatial resolution of 0.02 mm/pix were recorded at 5 frames per second. The centroid of each colony was obtained using the LabVIEW and Vision software (National Instruments), and the velocity of each colony was calculated from the displacement in 3 frames (0.6 s), leading to a lower limit of 0.033 mm/s for detecting the velocity.

For the light stimuli, the left and right sides of the chamber were illuminated using two halogen lamps. The optical axis coincided with the *x*-axis. The light was passed through dichroic filters such that light with a wavelength of 500–575 nm was used as the stimulus. The entire chamber was illuminated to reduce vertical movement of the colony. The light intensities I_R and I_L from the right and left sides were measured at the center of the chamber along the optical axis. In each trial, the colonies were stimulated using a rectangular wave with an amplitude of $|I_{dif}\ (=I_R - I_L)|$ and a period of 200 s for five periods. The velocity of the colony between 50 and 100 s after the sign of I_{dif} changed was calculated. To observe the photoresponse to the difference in relative light intensity, we varied I_{dif} for a given $I_{sum}(=I_R + I_L)$. When $I_{dif} = 0$ l×, small colonies at a high speed tended to move along the optical axis, whereas large colonies tended to move in random directions, and the photoresponses to I_{dif} were also different. Therefore, we analyzed the colonies with a speed ≤ 250 μm/s. All experiments were conducted in a dark room at 28 ± 2 °C. For initialization, *Volvox* colonies in the chamber were illuminated for 2.5 h at $I_{dif} = 0$ l× ($I_R = I_L = I_{sum}/2$) for a given I_{sum}. Because each somatic cell can detect the surrounding light during the colony's rotation, $I_{sum} = I_R + I_L$ can be considered as the light intensity of the surrounding environment for each somatic cell. Therefore, the initialization was performed under this condition, and subsequent experiments were conducted using the same I_{sum}.

Measuring the flow around an individual *Volvox* colony

A 1 mm-thick silicone rubber with an 18-mm diameter hole in the center was glued onto a glass slide. Next, 270 μL of *Volvox* solution with 2-μm diameter carboxylated polystyrene beads as tracer particles for PTV was placed into the sample cell. The height of the water layer is approximately 1 mm. *Volvox* colonies were captured by gently aspirating the posterior portion of each colony using a glass micropipette. The micropipettes were prepared by pulling them from the glass capillaries and inserting them into a holder. The colonies were held approximately 0.5-mm from the glass slide surface. Colonies with a diameter of 0.20–0.24 mm were selected as the typical size of mature colonies. The aspiration and movement of the micropipette holder were performed using a micromanipulator (NARISHIGE). Beads and colonies were observed using an inverted microscope (IX-73; Olympus) with a 10× objective lens under dark-field illumination consisting of red LEDs arranged in a circular pattern above the sample cell. The central wavelength was 630 nm, and *Volvox* showed a negligible response to red light. Green LEDs with a central wavelength of 525 nm were used as stimulus light. Four LEDs were installed near the condenser lens above the sample cell. The stimulus light was removed for observation by using a dichroic filter.

Images with a spatial resolution of 1.15 μm/pix were captured using a camera (IPX-VGA210-L; IMPERX) at 50 fps. In the PTV, beads in a rectangular area of 156 μm × 287 μm in front of the colony were analyzed because anterior somatic cells showed a greater response to light stimuli (30). Beads were traced from a series of images every 0.02 s, and their velocities were calculated from the 0.1 s displacements. These measurements were used to calculate the average speed of the beads in the rectangle.

During the first 10 s of each measurement, the intensity of the stimulating light was I_{before}, and then the intensity was changed to I_{after}. In free-swimming colonies, differences in light intensity were detected by rotation around the a–p axis. Thus, we regarded $I_{after} - I_{before}$ as I_{dif} and $I_{after} + I_{before}$ as I_{sum} for the immobilized colonies, corresponding to the phototaxis experiments for the colony population. We varied I_{dif} for a given I_{sum}. All experiments were conducted in a dark room at 28 ± 2 °C. For initialization, the *Volvox* colony in the sample cell was illuminated for 2.5 h at $I_{sum}/2$ for a given I_{sum}. To observe the response to different relative light intensities, I_{dif}/I_{sum}, I_{dif} were varied for each I_{sum}. Measurements were conducted for $I_{sum} = 1$, 200, 5, 100, and 9, 000 l×. Changes in light intensity, captured images, and PTV analysis were performed using the LabVIEW and Vision software (National Instruments).

Measuring the stop probability of flagellar beatings

A 0.13-mm-thick silicone sheet with a 5.5-mm diameter hole in the center was glued to a glass coverslip. The sample cell was filled with 4.5 μL of *Volvox* solution and covered with a glass coverslip. *Volvox* colonies were sandwiched between two coverslips, and colonies with a diameter of 0.20–0.24 mm and with their a–p axis in the *xy*-plane were selected for measurement. In a dark room at 28 ± 2 °C, all measurements were conducted within 90 min of sample preparation to minimize damage to the colonies. Images were acquired at different magnifications (4×, 10×, and 20×) to measure the angle θ from the anterior pole, and the θ was obtained from superimposed images as shown in Fig. 5A. Flagellar motion was observed using an inverted microscope with 20× objective lens and phase-contrast images were captured at 1,000 fps. The same microscope and camera were used for flow measurements.

The definitions of I_{before}, I_{after}, I_{dif}, and I_{sum} were the same as those used for the flow measurement. Similar to the flow measurements, the stimulus light intensity was set to I_{before} and then changed to I_{after} for the first 10 s of each measurement. The total observation time per trial was 30 s and the sample solution was illuminated at $I_{sum}/2$ for 80 s between trials. For the initialization, the *Volvox* solution was illuminated for 2.5 h at $I_{sum}/2$ for a given

I_{sum} before placing the solution in the sample cell. To observe the response to different relative light intensities, I_{dif}/I_{sum}, I_{dif} were varied for each I_{sum}. The measurements were conducted for I_{sum} = 1, 200, 2, 400, 3, 600, 5, 100, and 9, 000 l×. Changes in light intensity, captured images, and image analyses were performed using the LabVIEW, Vision, and ImageJ software (National Institutes of Health).

Acknowledgments

We thank N. Ueki for supplying *Volvox carteri* Eve10 and M. Yanagisawa for preparing the glass micropipettes.

Supplementary Material

Supplementary material is available at *PNAS Nexus* online.

Funding

This study was supported by JSPS KAKENHI (grant numbers 23740290 and 22H05067).

Author Contributions

Y.M. designed the study; K.H., Y.K., K.Y., T.I., M.O., and Y.M. performed the study; K.H. and Y.M. wrote the manuscript.

Data Availability

All data are included in the manuscript and/or supporting information.

References

1 De Maleprade H, Moisy F, Ishikawa T, Goldstein RE. 2020. Motility and phototaxis of Gonium, the simplest differentiated colonial alga. *Phys Rev E*. 101:022416.
2 Smith CL, Reese TS, Govezensky T, Barrio RA. 2019. Coherent directed movement toward food modeled in *Trichoplax*, a ciliated animal lacking a nervous system. *Proc Natl Acad Sci U S A*. 116: 8901–8908.
3 Davidescu MR, Romanczuk P, Gregor T, Couzin ID. 2023. Growth produces coordination trade-offs in *Trichoplax adhaerens*, an animal lacking a central nervous system. *Proc Natl Acad Sci U S A*. 120:e2206163120.
4 Cremer J, *et al*. 2019. Chemotaxis as a navigation strategy to boost range expansion. *Nature*. 575:658–663.
5 Tsang ACH, Lam AT, Riedel-Kruse IH. 2018. Polygonal motion and adaptable phototaxis via flagellar beat switching in the microswimmer *Euglena gracilis*. *Nat Phys*. 14:1216–1222.
6 Huang HW, Sakar MS, Petruska AJ, Pané S, Nelson BJ. 2016. Soft micromachines with programmable motility and morphology. *Nat Commun*. 7:12263.
7 Yasa O, Erkoc P, Alapan Y, Sitti M. 2018. Microalga-powered microswimmers toward active cargo delivery. *Adv Mat*. 30:1804130.
8 Wang J, *et al*. 2022. Volbots: *Volvox* microalgae-based robots for multimode precision imaging and therapy. *Adv Funct Mater*. 32: 2201800.
9 Ahmad R, *et al*. 2022. Bio-hybrid micro-swimmers propelled by flagella isolated from *C. reinhardtii*. *Soft Matter*. 18:4767–4777.
10 Sakaguchi H, Iwasa K. 1979. Two photophobic responses in *Volvox carteri*. *Plant Cell Physiol*. 20:909–916.
11 Hoops HJ. 1997. Motility in the colonial and multicellular Volvocales: structure, function, and evolution. *Protoplasma*. 199: 99–112.
12 Hoops HJ, Brighton MC, Stickles SM, Clement PR. 1999. A test of two possible mechanisms for phototactic steering in *Volvox carteri* (Chlorophyceae). *J Phycol*. 35:539–547.
13 Solari CA, Drescher K, Goldstein RE. 2011. The flagellar photoresponse in *Volvox* species (Volvocaceae, Chlorophyceae). *J Phycol*. 47:580–583.
14 Ueki N, Matsunaga S, Inouye I, Hallmann A. 2010. How 5000 independent rowers coordinate their strokes in order to row into the sunlight: phototaxis in the multicellular green alga *Volvox*. *BMC Biol*. 8:103.
15 Kirk DL. 1998. *Volvox: molecular-genetic origins of multicellularity and cellular differentiation*. Cambridge University Press.
16 Kirk DL. 2001. Germ-soma differentiation in *Volvox*. *Dev Biol*. 238: 213–223.
17 Kirk DL, Nishii I. 2001. *Volvox* carteri as a model for studying the genetic and cytological control of morphogenesis. *Dev Growth Differ*. 43:621–631.
18 Nishii I, Miller SM. 2010. *Volvox*: simple steps to developmental complexity? *Curr Opin Plant Biol*. 13:646–653.
19 Umen JG. 2020. *Volvox* and volvocine green algae. *Evodevo*. 11:13.
20 Drescher K, *et al*. 2009. Dancing *Volvox*: hydrodynamic bound states of swimming algae. *Phys Rev Lett*. 102:168101.
21 Drescher K, Goldstein RE, Michel N, Polin M, Tuval I. 2010. Direct measurement of the flow field around swimming microorganisms. *Phys Rev Lett*. 105:168101.
22 Rushkin I, Kantsler V, Goldstein RE. 2010. Fluid velocity fluctuations in a suspension of swimming protists. *Phys Rev Lett*. 105: 188101.
23 Brumley DR, Wan KY, Polin M, Goldstein RE. 2014. Flagellar synchronization through direct hydrodynamic interactions. *Elife*. 3: e02750.
24 Goldstein RE. 2015. Green algae as model organisms for biological fluid dynamics. *Annu Rev Fluid Mech*. 47:343–375.
25 Foster KW, Smyth RD. 1980. Light antennas in phototactic algae. *Microbiol Rev*. 44:572–630.
26 Hegemann P. 1997. Vision in microalgae. *Planta*. 203:265–274.
27 Kreimer G. 2009. The green algal eyespot apparatus: a primordial visual system and more? *Curr Genet*. 55:19–43.
28 Ebnet E, Fischer M, Deininger W, Hegemann P. 1999. *Volvox* rhodopsin, a light-regulated sensory photoreceptor of the spheroidal green alga *Volvox carteri*. *Plant Cell*. 11:1473–1484.
29 Ueki N, Wakabayashi K. 2018. Detergent-extracted *Volvox* model exhibits an anterior–posterior gradient in flagellar Ca^{2+} sensitivity. *Proc Natl Acad Sci U S A*. 115:E1061–E1068.
30 Drescher K, Goldstein RE, Tuval I. 2010. Fidelity of adaptive phototaxis. *Proc Natl Acad Sci U S A*. 107:11171–11176.
31 Ozaki M, Murayama Y. 2015. Fluctuations and responses in stochastic motions of *Volvox* colonies. *Curr Phys Chem*. 5:64–72.